Holocene dynamics of the Arctic's largest ice shelf

Dermot Antoniades[a,1,2], Pierre Francus[a,b,c], Reinhard Pienitz[a], Guillaume St-Onge[c,d], and Warwick F. Vincent[a]

[a]Centre d'études nordiques, Université Laval, Québec, QC, Canada G1V 0A6; [b]Institut National de la Recherche Scientifique: Eau, Terre et Environnement, Québec, QC, Canada G1K 9A9; [c]GEOTOP Research Center, Montréal, QC, Canada H3C 3P8; and [d]Institut des sciences de la mer de Rimouski, Rimouski, QC, Canada G5L 3A1

Edited by Eugene Domack, Hamilton College, Clinton, NY, and accepted by the Editorial Board September 21, 2011 (received for review April 20, 2011)

Ice shelves in the Arctic lost more than 90% of their total surface area during the 20th century and are continuing to disintegrate rapidly. The significance of these changes, however, is obscured by the poorly constrained ontogeny of Arctic ice shelves. Here we use the sedimentary record behind the largest remaining ice shelf in the Arctic, the Ward Hunt Ice Shelf (Ellesmere Island, Canada), to establish a long-term context in which to evaluate recent ice-shelf deterioration. Multiproxy analysis of sediment cores revealed pronounced biological and geochemical changes in Disraeli Fiord in response to the formation of the Ward Hunt Ice Shelf and its fluctuations through time. Our results show that the ice shelf was absent during the early Holocene and formed 4,000 years ago in response to climate cooling. Paleoecological data then indicate that the Ward Hunt Ice Shelf remained stable for almost three millennia before a major fracturing event that occurred ~1,400 years ago. After reformation ~800 years ago, freshwater was a constant feature of Disraeli Fiord until the catastrophic drainage of its epishelf lake in the early 21st century.

climate change | glaciology | paleoceanography | geochemistry

Robert Peary's expedition in 1906 described a "broad glacial fringe" (i.e., an ice shelf) covering much of the coast of northwestern Ellesmere Island (1) that may have been as large as 8,900 km^2 (2). The first maps of the extent of these ice shelves were made from aerial and ground surveys during the 1950s and implied significant reductions in ice extent (3, 4). By the end of the 20th century, melting and calving had reduced this single ice shelf to six isolated fragments encompassing less than 1,043 km^2, and deterioration over the last decade has eliminated another ~300 km^2, including the complete loss of the Ayles and Markham ice shelves (2, 5) (Fig. 1). The Ward Hunt Ice Shelf (WHIS) is the largest remaining Arctic ice shelf, with an area of ~400 km^2 (6). Disintegration of northern ice shelves has paralleled large reductions in Arctic Ocean ice that have led to the conjecture that ice-free conditions are possible in the near future (7–9).

Arctic ice shelves are formed mainly from the thickening over time of landfast sea ice, in contrast to Antarctic ice shelves, which are typically floating extensions of continental glaciers. In locations where ice shelves block fiord mouths, they dam inflowing freshwater and produce density-stratified ecosystems, known as epishelf lakes, in which a freshwater layer is superimposed on denser ocean waters. Because these lakes cannot form in the absence of ice shelves, their existence provides direct evidence of intact ice shelves, and their sedimentary records represent potential continuous archives of past ice-shelf dynamics (10). A 4.0-km^3 epishelf lake was retained within Disraeli Fiord by the WHIS until its catastrophic drainage in 2001 (11).

Estimates of the age of the WHIS have hitherto been based on radiocarbon-dated driftwood found behind the ice shelf's modern margins. These studies suggested ice-shelf absence after deglaciation at ~9.5 calibrated (cal) ka BP and produced a range of WHIS age estimates between 3.0 and 5.5 cal ka BP (12–16). Although the presence of ice shelves precludes driftwood emplacement, it is difficult to ascertain whether periods of driftwood absence may have been caused by ice shelves or by past variability in delivery mechanisms such as ocean currents or ice conditions, changes in terrestrial vegetation, or potential disturbance after deposition (17, 18); driftwood-based dates are consequently recognized as providing only upper limits to ice-shelf ages (12, 18, 19). The history of the ice shelves of northern Ellesmere Island and the significance of their recent decline therefore remains unclear. Here we present a continuous paleoenvironmental reconstruction of conditions within the water column of Disraeli Fiord, where changes directly caused by the WHIS were recorded by a series of biological and geochemical proxy indicators.

Results

Obvious shifts in proxy indicators in the Disraeli Fiord sedimentary record during the >8,000 years encompassed by the cores (Fig. 2) reflect fundamental changes in fiord conditions caused by the presence or absence of an ice shelf (Figs. 3 and 4). X-radiographs and Al:Ti ratios indicated that these shifts could not be attributed to changes in core lithology or sediment provenance (Fig. S1). One group of proxy indicators, including magnetic susceptibility, pigment ratios, and foraminiferal concentrations, displayed clear and consistent responses to WHIS presence/absence (Fig. 4). A second group, including Mn:Fe ratios, total organic carbon (TOC), total inorganic carbon (TIC), and Sr:Ca ratios were more sensitive to the effects of mid-Holocene sediment reoxygenation; this group consistently tracked shifts between marine and freshwater conditions in Disraeli Fiord, but their values varied between early Holocene anoxic and late-Holocene oxic marine phases (Fig. 3). Diatoms were almost entirely absent throughout the sedimentary sequence, consistent with samples taken from the Disraeli Fiord water column during the last decade, in which they were extremely rare.

Discussion

The sedimentary record indicates three distinct states in Disraeli Fiord during the Holocene (Figs. 3 and 4): (*i*) ice-shelf absence, characterized by marine, strongly ice-covered fiord waters, extremely low productivity, and anoxic sediments; (*ii*) ice-shelf–induced epishelf conditions, indicated by freshwater pigment signatures, greater retention of allochthonous sediment inputs, and moderately higher biomass and paleoproductivity; and (*iii*) open marine conditions indicative of ice-shelf fracturing, characterized by marine pigment signatures, low sediment retention, and relatively high biomass.

Geochemical data suggest that Disraeli Fiord was an ice-dominated marine environment during the early Holocene, isolated from the atmosphere by heavy ice cover (Fig. 3). Although

Author contributions: D.A. and W.F.V. designed research; D.A., P.F., G.S.-O., and W.F.V. performed research; D.A., P.F., R.P., G.S.-O., and W.F.V. analyzed data; and D.A., P.F., R.P., G.S.-O., and W.F.V. wrote the paper.

The authors declare no conflict of interest.

This article is a PNAS Direct Submission. E.D. is a guest editor invited by the Editorial Board.

[1]Present address: Sección Limnología, Facultad de Ciencias, Universidad de la República, Iguá 4225, Montevideo, 11400, Uruguay.

[2]To whom correspondence should be addressed. E-mail: dermot.antoniades@cen.ulaval.ca.

This article contains supporting information online at www.pnas.org/lookup/suppl/doi:10.1073/pnas.1106378108/-/DCSupplemental.

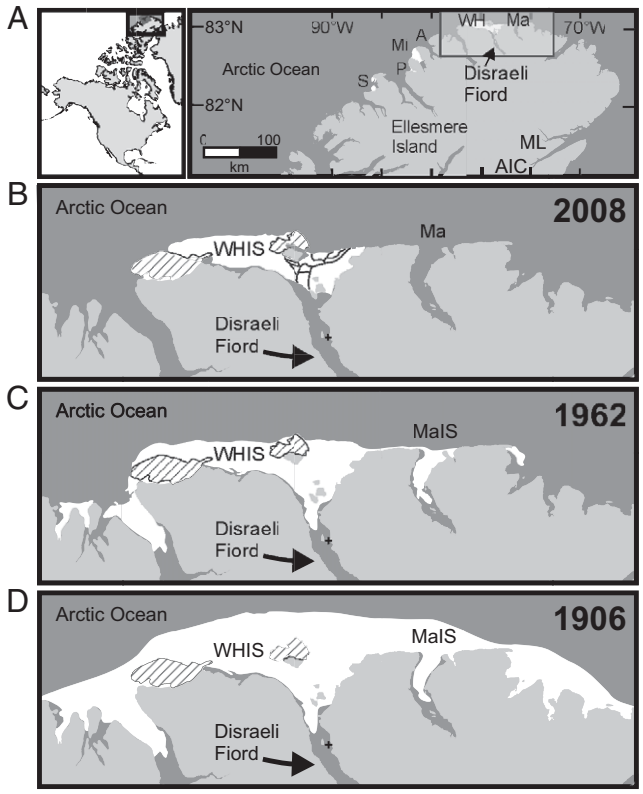

Fig. 1. The ice shelves of northern Ellesmere Island in 2008 (*A* and *B*) and changes in the margin of the WHIS during the 20th century. The data from 1962 (*C*) and 1906 (*D*) are from refs. 51 and 52, respectively. The hatched white areas represent ice rises, the plus sign in Disraeli Fiord is the coring location, and the thin lines on the WHIS in *B* indicate fractures present after summer 2008. S, Serson Ice Shelf; P, Petersen Ice Shelf; Mi, Milne Ice Shelf; A, Ayles Ice Shelf; Ma, Markham Ice Shelf; AIC, the northern margin of the Agassiz Ice Cap; ML, Murray Lake.

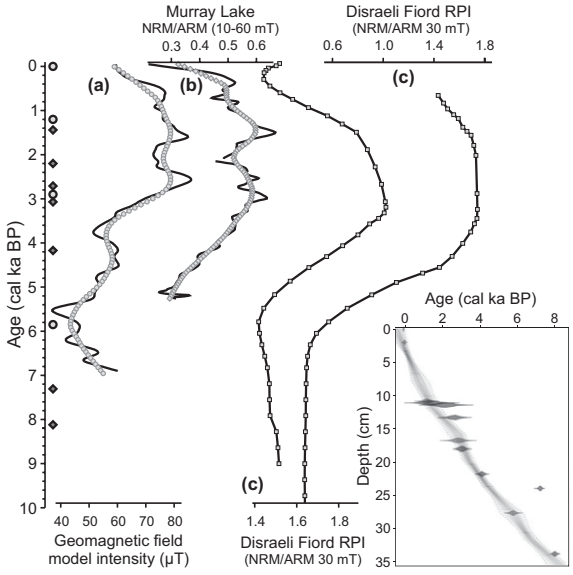

Fig. 2. Age–depth model and correlation of Disraeli Fiord to regional paleomagnetic records. (*A*) Geomagnetic field model output (46) and smoothed curve (○). (*B*) Relative paleointensity (RPI) from Murray Lake, Ellesmere Island (45) and smoothed curve (♢). (*C*) RPI of overlapping Disraeli Fiord core sections (□). Symbols along the *y* axis represent ^{14}C dates (♢) and paleomagnetic tie points (i.e., inflection points in paleomagnetic data where our records were tied to published curves; ○) used in age–depth model construction. (*Inset*) Bayesian age–depth model.

the fiord was not occupied by glaciers during the last glaciation, sea ice that may have exceeded 40-m thickness is thought to have characterized the region (15, 20). Such thick sea ice would have placed strong constraints on photosynthesis and exchange with the atmosphere; over the course of centuries to millennia, such isolation would be conducive to oxygen depletion. Geochemical characteristics of the sediment corroborate this hypothesis, with Mn concentrations in the early to mid-Holocene indicative of Mn reduction under anoxic bottom water conditions (Fig. 3*A*) (21). Low Mn:Fe ratios (Fig. 3*A*) also indicate limited ventilation, as reported elsewhere in the Arctic Ocean below glacial ice (22). The suppression of biological activity in the early Holocene by thick ice is reflected by sediment pigment concentrations below detection limits (Fig. 3*F*) and extremely low TOC content ($\bar{x}$ = 0.21%, σ = 0.02%; Fig. 3*C*). Depleted carbon isotope composition of organic carbon ($\delta^{13}C_{ORG}$) values (Fig. 3*D*) were typical of phytoplankton in subzero waters and reflect high dissolved inorganic CO_2 (ΣCO_2) caused by low temperatures and thick ice (23, 24), whereas the early Holocene paucity of foraminifera [2-43 tests per gram of dry weight (g.d.w.)$^{-1}$] likely results from bottom anoxia, limited food supply because of low phytoplankton biomass, or a combination of these factors and mirrors near-absences observed in the Arctic Ocean under heavy ice (25).

There was no indication of ice-shelf presence during the early to mid-Holocene, and multiple lines of evidence suggest gradual early Holocene ice retreat in Disraeli Fiord in response to the warm temperatures recorded in nearby ice cores (26, 27). Inferences from the sedimentary record regarding the timing of deglaciation are limited by a lack of firm age control before ∼8.7 cal ka BP; regionally, however, ice recession was surmised to have begun ∼9.5 cal ka BP, and driftwood penetration into Disraeli Fiord was recorded from ∼9.2 cal ka BP onward to the mid-Holocene (12, 15, 16, 19). The appearance of detectable pigments in sediments ∼6.2 cal ka BP suggests diminishing severity of below-ice conditions, and the absence of epishelf conditions in the photic zone is implied by low chlorophyll (chl)-*b*:*a* ratios characteristic of polar marine environments (28, 29). Low magnetic susceptibility and Ti content in the early Holocene also indicate limited retention of allochthonous minerogenic material (Figs. 3*B* and 4*A*). Altogether, these characteristics suggest limited summer ice melt and preclude the presence of a fully formed ice dam, whereas evidence of sea-ice push near the marine limit confirms that Disraeli Fiord sustained significant ice cover during this time (15).

Progressive changes in Disraeli Fiord sediments indicate cooling climates during the mid-Holocene. After ∼5.0 ka BP, thickening coastal sea ice began to retain sediment inputs, as reflected by increases in magnetic susceptibility and Ti content (Figs. 3*B* and 4*A*), although chl-*b*:*a* ratios imply that the surface waters remained marine. Sharp shifts in Mn:Fe ratios (Fig. 3*A*) suggest that entrainment through the water column of this sediment-laden, oxygen-rich meltwater reoxygenated the fiord floor beginning ∼4.8 cal ka BP, and the colonization of these newly oxic sediments by benthic foraminifera is indicated by significantly higher abundances after this time ($P < 0.001$; Fig. 4*D*). The lag between cores in the onset of oxygenation of the sediments (Fig. 3*A*), resulting from different water depths (i.e., 55 vs. 69 m), is consistent with downward mixing of oxygen through the fiord.

Profound environmental change in Disraeli Fiord associated with the transition to an ice-dammed freshwater ecosystem is marked by shifts in the sedimentary record ∼4.0 cal ka BP (Fig. 4). These shifts are coincident with the inception of minimum

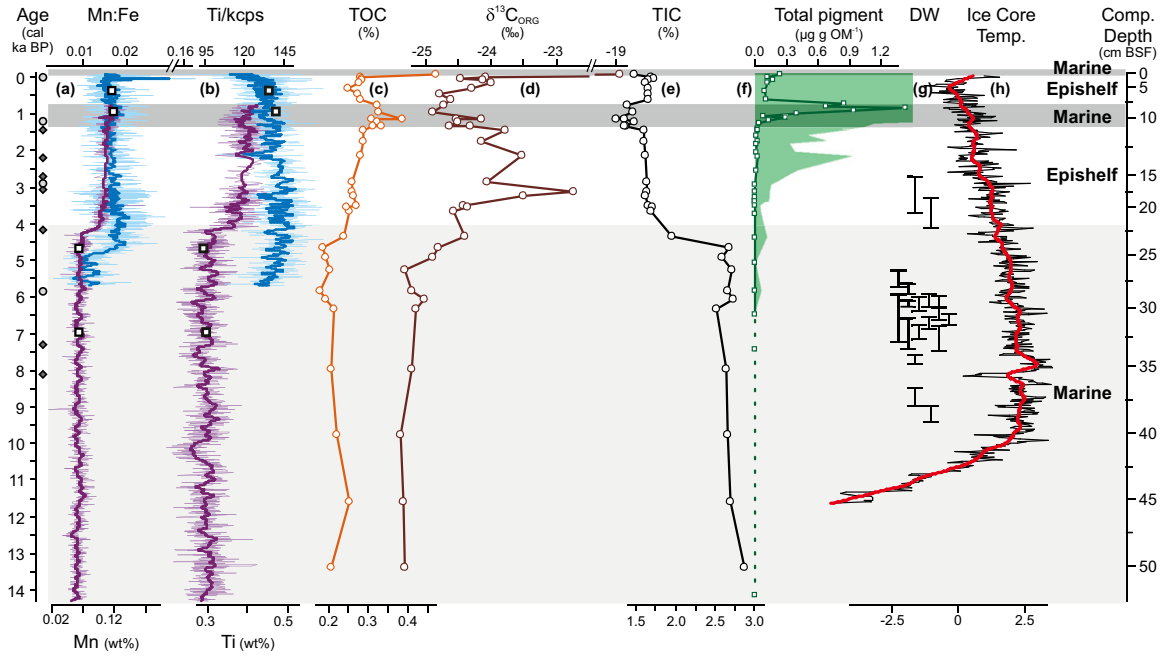

Fig. 3. Holocene profiles of sediment indicators in Disraeli Fiord. (*A*) Mn:Fe (XRF ratios: curves, upper *x* axis) and Mn concentration (ICP-AES: □, lower *x* axis). (*B*) Ti (XRF counts·s^{-1} divided by total kilocounts·s^{-1}: curves, upper *x* axis) and ICP-AES concentrations (□, lower *x* axis). XRF data: blue lines represent the upper core section taken at 55-m depth, and purple lines indicate the lower section from 69-m depth. The thin lines represent the raw data measured at 200-μm intervals and the thicker, darker lines are locally weighted scatterplot smoothing (LOESS)-smoothed curves. (*C*) Percentage TOC. (*D*) $\delta^{13}C_{ORG}$ (vs. Vienna Pee Dee Belemnite). (*E*) Percentage TIC. (*F*) Total pigment concentration, where the shaded area represents a 30× exaggeration to show trends in low concentration samples. (*G*) The 2σ-calibrated ^{14}C age ranges for driftwood samples from Disraeli Fiord (ref. 16 and refs. therein). (*H*) Ellesmere Island/Greenland composite Holocene ice-core temperature record (53). Symbols along the left *y* axis represent ^{14}C dates (◇) and paleomagnetic tie points (○) used in age–depth model construction (*Materials and Methods*). Comp. depth, composite core depth (in cm) below sea floor.

summer melt in Ellesmere Island ice-cap records (26), the end of optimum Holocene temperatures in Greenland (27), and records from northern Greenland that suggest less sea ice than at present until at least 4.5 cal ka BP (30). The increasing isolation of the fiord from the Arctic Ocean is recorded by indicators of allochthonous retention (i.e., magnetic susceptibility, Ti), whereas pigment data provide evidence for the establishment of stratification attributable to the damming of freshwater. Pigment shifts indicated greater freshwater presence because chl-*b*:*a* ratios increased significantly ($P < 0.05$) from marine values to those typical for epishelf and polar meromictic lakes, reflecting the greater importance of chlamydomonads and other Chlorophyta in freshwater communities with dominant ice-cover regimes (29). Paleoproductivity indicators, including sediment pigment concentrations and TOC, suggested moderately higher biomass in Disraeli Fiord in response to the retention of nutrient inputs behind the ice dam, whereas Sr:Ca ratios, which have been suggested to record paleoproductivity (31), mirrored these trends (Fig. 4*E*). Meanwhile, foraminiferal abundances increased sharply; their significant correlation with pigment concentrations ($r = 0.76$, $P < 0.001$) suggested that they were responding to greater phytoplankton food supply. $\delta^{13}C_{ORG}$ also differed significantly ($P = 0.05$) between marine and epishelf stages, with higher $\delta^{13}C_{ORG}$ values after ∼4 cal ka BP reflective of the accumulation of ^{13}C-rich meltwater behind the ice shelf (10). One Disraeli Fiord driftwood sample had a ^{14}C range that fell after the sediment-inferred date of ice-shelf formation (12) (Fig. 3*G*); if correct, this occurrence may imply a degree of instability in the nascent ice shelf.

The WHIS was then largely stable for three millennia until it underwent a period of degradation at ∼1.4 cal ka BP, when it was unable to retain freshwater for several centuries. The fracturing of the ice shelf and a shift from epishelf to marine conditions was recorded by the pronounced reduction of chl-*b*:*a* ratios to distinctly marine values (Fig. 4*B*). Sharply lower magnetic susceptibility and Ti content further indicated that allochthonous inputs were no longer retained behind an ice dam, and lower $\delta^{13}C_{ORG}$ reflected the increasing influence of marine organic matter, as observed in analogous Antarctic ecosystems (10) (Fig. 3*D*). Higher biomass resulting from reduced ice cover and warmer conditions was indicated by spikes in sediment pigment concentrations and Sr:Ca ratios as well as higher TOC concentrations (Figs. 3 and 4). Disraeli Fiord changes mirrored trends in regional paleoclimate records, and together they suggest that conditions were conducive to loss of ice-shelf integrity at this time. Winter temperatures recorded in Greenland ice cores from 1.3–0.9 ka BP were comparable to those that caused recent ice-shelf fracturing (32) (Fig. 4*F*), and a period of minimum sea-ice extent at 1.5–0.8 cal ka BP in the central Canadian Arctic Archipelago was recorded by marine biomarker records (33) (Fig. 4*C*). Moreover, driftwood delivery to northern Greenland marked the removal of landfast sea ice at ∼1.2–0.6 ka BP (30). Although it was suggested that this period occurred during more than two millennia of "dramatic centennial fluctuations" in Greenland perennial landfast ice beginning at ∼2.5 cal ka BP (30), our data suggest only a single episode of WHIS instability between 1.4 and 0.8 cal ka BP.

The WHIS reformed at 0.8 cal ka BP because of cooling temperatures. Beginning at ∼1.0 cal ka BP, shifts in magnetic susceptibility (Fig. 4*A*) suggest increased retention by thickening sea ice, paralleling $\delta^{18}O$ decreases in Greenland ice cores (32) (Fig. 4*F*). The establishment of the Disraeli epishelf lake is recorded by sharp shifts in pigment ratios after ∼0.8 cal ka BP (Fig. 4*B*), whereas reductions in productivity under increasing ice cover are reflected by lower pigment concentrations, TOC, and Sr:Ca ratios (Figs. 3 *C* and *F* and 4*E*). After this time, pigment

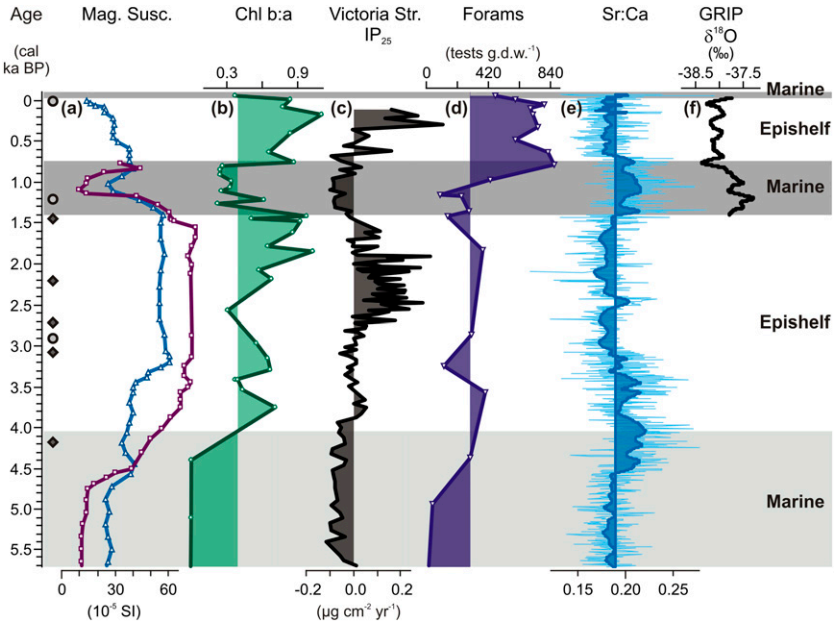

Fig. 4. Indicators of epishelf conditions from 5.7 cal ka BP to present. (*A*) Magnetic susceptibility from two overlapping core sections. (*B*) Chl-*b*:*a* calculated as the ratio of the sum of chl-*b* and degradation products to total chl-*a* and degradation products. (*C*) IP_{25} sea-ice biomarker record from the central Canadian Arctic Archipelago (33). (*D*) Forams: sediment foraminiferal abundances. (*E*) Sr:Ca ratios (Itrax). Light blue line, raw data; blue line, locally weighted scatterplot smoothing (LOESS)-smoothed data. (*F*) Greenland Ice Core Project (GRIP) ice-core winter $\delta^{18}O$ temperature proxy (32). Magnetic susceptibility records are from both core sections, Sr:Ca ratio is taken from the upper core section alone, and other records are composites from the overlapping core sections (*SI Materials and Methods*). The shading represents deviations from the median for the last 5.0 cal ka BP, except for chl-*b*:*a* (*B*), whose value (0.4) represents the transition between ratios indicative of Arctic freshwater and marine phytoplankton communities. Symbols along the left *y* axis represent ^{14}C dates (◇) and paleomagnetic tie points (○) used in age–depth model construction.

proxies indicate stability of the WHIS and increasing freshwater influence until 20th century changes, although the presence of abundant foraminifera throughout this stage implies that the deep bottom waters of Disraeli Fiord remained marine at all times.

Recent WHIS fragmentation is recorded in the uppermost sediments. Water column profiles taken from Disraeli Fiord indicate that roughly half of the volume of the epishelf lake was lost between 1954, when it was first identified, and 1999 (11, 34). The prominent changes near the sediment surface therefore include longer-term effects of climate change that predate the catastrophic drainage of the epishelf lake in 2001–2002. Increasing marine influence attributable to the shrinking and eventual disappearance of the epishelf lake is recorded by lower chl-*b*:*a* ratios (Fig. 4*B*), whereas higher TOC and pigment concentrations reflect greater productivity resulting from 20th century warming (Fig. 3 *C* and *F*). Although sharp shifts in elementary concentrations were evident at the sediment surface, we interpret them cautiously given their occurrence in the redox zone (i.e., above the sharp Mn peaks in Fig. 3). The return to lower magnetic susceptibility values and, to a lesser extent, Ti content, again reflects the loss of allochthonous inputs to the Arctic Ocean in the absence of an intact ice shelf. The sharp shift toward less depleted $\delta^{13}C_{ORG}$ at the surface may reflect an increase in the contribution of sea-ice algae that became established after the return of marine conditions and that prospered because relatively thin ice permitted greater penetration of solar radiation (35).

The Holocene record of Antarctic ice shelves may provide additional insight into Arctic ice-shelf dynamics. Although their different origins complicate such comparisons, numerous ice shelves in both hemispheres have degraded rapidly in response to recent warming. Studies from the Antarctic Peninsula indicate asynchronous change during the Holocene and suggest a relationship between ice-shelf size and sensitivity to collapse. Larsen B Ice Shelf was present throughout the Holocene (36), whereas George VI Ice Shelf was absent only during maximum Holocene warmth at ∼9.6–7.9 cal ka BP (37). Other, smaller systems were absent for longer mid-Holocene periods before recent collapse, including the Müller (38), Prince Gustav Channel (39), and Larsen A (40) ice shelves, suggesting a need for studies of smaller Arctic ice-shelf systems to determine whether they too display heightened sensitivity to past climate shifts.

The Disraeli Fiord sediment record indicates a stable WHIS from 0.8 cal ka BP (i.e., 1150 A.D.) until its recent disintegration. Although indicators including TOC and $\delta^{13}C_{ORG}$ reached extreme values at the sediment surface, modern measures of other proxies were within their Holocene ranges. It is therefore uncertain whether current environmental conditions exceed natural variability, and future monitoring of the Disraeli Fiord ecosystem will be crucial in resolving this question. Our findings imply that the recent collapse of northern ice shelves cannot be considered unprecedented, with evidence of at least some fracturing and break-up of the coastal fringe of thick ice at ∼1.4 cal ka BP that resulted in the drainage of the Disraeli Fiord epishelf lake. However, the results also indicate that ice-shelf integrity was subsequently reestablished and that the WHIS has been present for the majority of the last 4,000 years. The break-up of the WHIS and associated loss of the epishelf lake at the turn of the 21st century is therefore a significant event at the millennial scale and suggests that current climates at the northern limit of North America are at their warmest in nearly 1,000 years.

Materials and Methods

Sediment cores were taken from Disraeli Fiord, located behind the WHIS, through the ice along a transect from 82° 52′ 21″N, 73° 29′ 18″W to 82° 52′ 22″N, 73° 28′ 54″W from May 31 to June 7, 2006, with a combined gravity/percussion corer (Aquatic Research Instruments). Four cores between 17 and 47 cm in length were retrieved in water depths from 48 to 69 m, sealed immediately, and transported intact, cold, and in the dark to the laboratory.

The two longest cores (38 and 47 cm), taken in 55 and 69 m of water, respectively, were split lengthwise, with one half used for pigment analysis and the other for analysis of paleomagnetic properties, elemental geochemistry, C and N, $\delta^{13}C_{ORG}$, and foraminifera (*SI Materials and Methods* and Figs. S1 and S2). Both cores were composed of massive silty clay with diffuse color banding from brownish yellow to greenish gray (*SI Materials and Methods*). Correlation of the overlapping core sections was performed by using magnetic susceptibility data and refined with the high-resolution Ti and Al stratigraphy. These analyses indicated an absence of the uppermost sediments in one core section and an intact sediment-water interface in the other (Fig. S2).

Pigments were analyzed with reverse-phase HPLC. Extraction, solvent, and quantification protocols followed those of Zapata et al. (41) and Antoniades et al. (42) (but also see *SI Materials and Methods*), and concentrations are expressed relative to organic matter content (ng g^{-1} OM^{-1}) determined by loss on ignition at 550 °C. Geochemical sediment characteristics were measured on an Itrax X-ray fluorescence (XRF) core scanner equipped with a 3-kW Mo tube, using an interval of 200 μm and an exposure time of 10 s; element contents are expressed as counts per second. Four discrete samples were analyzed for 18 major, minor, and trace elements by inductively coupled plasma/atomic emission spectrometry (ICP-AES) with a Varian Vista AX CCD Simultaneous ICP-AES, Palo Alto model, to validate results obtained by the XRF scanner.

C and N were analyzed by high-temperature catalytic combustion with an NC Instruments 2500 elemental analyzer, with carbonates removed by acidification before analysis of organic carbon (TOC). Stable isotope analysis of organic carbon was performed with a Micromass Isoprime isotope ratio mass spectrometer coupled with a Vario MICRO Cube elemental analyzer; ratios are expressed in δ notation relative to the standard Vienna Pee Dee Belemnite. Differences in mean $\delta^{13}C_{ORG}$ between sample groups were evaluated with one-way analysis of variance using the Holm–Sidak method for multiple pairwise comparisons. Fossil foraminifera samples were weighed, wet-sieved at 63 μm, and enumerated under a binocular microscope. Magnetic susceptibility was measured with a Bartington MS2E high-resolution sensor. Stratigraphic zones were determined with the computer program PSIMPOLL 4.26 (43) using optimal splitting, and only significant zones are reported. Because of differences in sampling resolution, zones were calculated separately for XRF data, pigments, and carbon variables and retained only if indicated in at least two of three datasets. Zone boundaries were averaged where they differed slightly because of variable sampling intervals and were rounded to the nearest hundred years.

Age–depth relationships were modeled with a combination of paleomagnetic and radiocarbon dating techniques. Relative paleointensity (RPI) was determined by following the methods of Barletta et al. (44), correlated to nearby records from a varved lake from Ellesmere Island and geomagnetic field model output (45, 46), and then validated and augmented with seven radiocarbon ages. Samples submitted for accelerator mass spectrometry (AMS) radiocarbon dating were prepared at the Université Laval Radiocarbon Laboratory and analyzed at the Keck Carbon Cycle AMS Facility (Irvine, CA) or Beta Analytic (Miami, FL) (Table S1). The age–depth model (Fig. 2) was constructed by using Markov chain Monte Carlo Bayesian methods based on seven AMS dates of hand-picked foraminiferal ^{14}C and four unambiguous inflection points where our RPI record was tied to published paleomagnetic curves (45, 46) (*SI Materials and Methods* and Table S2). All dates presented are calibrated with the Marine09 dataset (47), with a local ΔR of 335 ± 85 years applied to all samples (48) and an additional variable carbon reservoir within epishelf stages assuming a fixed carbon pool because of isolation by the strong perennial ice cover (49, 50) (*SI Materials and Methods* and Table S1). Ages beyond the lowest accepted ^{14}C sample were calculated by extrapolation of the sedimentation rate of the lowest model section. Three questionable ^{14}C samples were excluded from the age–depth model (*SI Materials and Methods*).

ACKNOWLEDGMENTS. We thank Charles Gobeil, Jean-Pierre Guilbault, and Roberto Quinlan for stimulating discussions; Jean-François Hélie (GEOTOP) for carbon measurements; and Simon Belt for providing sea-ice biomarker data. D. Sarrazin, J. Tomkins, and E. Bottos assisted in coring operations. Our thanks go to Parks Canada for their support and cooperation as well as to the Polar Continental Shelf Program (Natural Resources Canada) for logistical support. We appreciate the thorough reviews by two anonymous reviewers. This work was supported by the Natural Sciences and Engineering Research Council of Canada, the Fonds Québécois de la Recherche sur la Nature et les Technologies, the Network of Centres of Excellence of Canada program ArcticNet, and the Canada Research Chairs program. This is a contribution to the Centre d'études nordiques (CEN) long-term program Northern Ellesmere Island in the Global Environment (NEIGE) and Polar Continental Shelf Program Contribution 032-11.

1. Peary RE (1907) *Nearest the Pole. A Narrative of the Polar Expedition of the Peary Arctic Club in the S. S. Roosevelt, 1905–1906* (Hutchinson, London).
2. Vincent WF, Gibson JAE, Jeffries MO (2001) Ice shelf collapse, climate change and habitat loss in the Canadian High Arctic. *Polar Rec (Gr Brit)* 37:133–142.
3. Dunbar M, Greenaway KR (1956) *Arctic Canada from the Air* (Canada Defence Research Board, Ottawa).
4. Crary AP (1956) Geophysical studies along northern Ellesmere Island. *Arctic* 9:154–165.
5. Copland L, Mueller DR, Weir L (2007) Rapid loss of the Ayles Ice Shelf, Ellesmere Island, Canada. *Geophys Res Lett* 34:L21501.
6. Mueller DR, Copland L, Hamilton A, Stern D (2008) Examining Arctic ice shelves prior to the 2008 breakup. *Eos Trans AGU* 89:502–503.
7. Holland MM, Bitz CM, Tremblay B (2006) Future abrupt reductions in the summer Arctic sea ice. *Geophys Res Lett* 33:L23503.
8. Maslanik J, et al. (2007) A younger, thinner arctic ice cover: Increased potential for rapid, extensive sea-ice loss. *Geophys Res Lett* 34:L24501.
9. Eisenman I, Wettlaufer JS (2009) Nonlinear threshold behavior during the loss of Arctic sea ice. *Proc Natl Acad Sci USA* 106:28–32.
10. Smith JA, et al. (2006) Limnology of two Antarctic epishelf lakes and their potential to record periods of ice shelf loss. *J Paleolimnol* 35:373–394.
11. Mueller DR, Vincent WF, Jeffries MO (2003) Break-up of the largest Arctic ice shelf and associated loss of an epishelf lake. *Geophys Res Lett* 30:2031.
12. Crary AP (1960) Arctic ice island and ice shelf studies. Part II. *Arctic* 13:32–50.
13. Lyons JB, Mielke JE (1973) Holocene history of a portion of northernmost Ellesmere Island. *Arctic* 26:314–323.
14. Stewart TG, England JH (1983) Holocene sea-ice variations and paleoenvironmental change, northernmost Ellesmere Island, NWT, Canada. *Arct Alp Res* 15:1–17.
15. Lemmen DS (1989) The last glaciation of Marvin Peninsula, northern Ellesmere Island, High Arctic, Canada. *Can J Earth Sci* 26:2578–2590.
16. England JH, et al. (2008) A millennial-scale record of Arctic Ocean sea ice variability and the demise of the Ellesmere Island ice shelves. *Geophys Res Lett* 35:L19502.
17. Dyke AS, England JH, Reimnitz E, Jetté H (1997) Changes in driftwood delivery to the Canadian Arctic Archipelago: The hypothesis of postglacial oscillations of the Transpolar Drift. *Arctic* 50:1–16.
18. Bradley RS (1990) Holocene paleoclimatology of the Queen Elizabeth Islands, Canadian High Arctic. *Quat Sci Rev* 9:365–384.
19. Blake W, Jr. (1972) Climatic implications of radiocarbon-dated driftwood in the Queen Elizabeth Islands, Arctic Canada. *Climatic Changes in Arctic Areas During the Last Ten-Thousand Years*, eds Vasari Y, Hyvärinen H, Hicks S (University of Oulu, Oulu, Finland), pp 77–104.
20. Bradley RS, England JH (2008) The Younger Dryas and the sea of ancient ice. *Quat Res* 70:1–10.
21. Crusius J, Calvert S, Pedersen T, Sage D (1996) Rhenium and molybdenum enrichments in sediments as indicators of oxic, suboxic and sulfidic conditions of deposition. *Earth Planet Sci Lett* 145:65–78.
22. Löwemark L, Jakobsson M, Mörth M, Backman J (2008) Arctic Ocean manganese contents and sediment colour cycles. *Polar Res* 27:105–113.
23. Rau GH, Takahashi T, Des Marais DJ (1989) Latitudinal variations in plankton δ ^{13}C: Implications for CO_2 and productivity in past oceans. *Nature* 341:516–518.
24. Meyers PA (1997) Organic geochemical proxies of paleoceanographic, paleolimnologic, and paleoclimatic processes. *Org Geochem* 27:213–250.
25. Darby DA, Polyak L, Bauch HA (2006) Past glacial and interglacial conditions in the Arctic Ocean and marginal seas—a review. *Prog Oceanogr* 71:129–144.
26. Fisher DA, Koerner RM, Reeh N (1995) Holocene climatic records from Agassiz Ice Cap, Ellesmere Island, NWT, Canada. *Holocene* 5:19–24.
27. Johnsen SF, et al. (2001) Oxygen isotope and paleotemperature records from six Greenland ice-core stations: Camp Century, Dye-3, GRIP, GISP2, Renland and NorthGRIP. *J Quat Sci* 16:299–307.
28. Trees CC, Clarke DK, Bidigare RR, Ondrusek ME, Mueller JL (2000) Accessory pigments versus chlorophyll a concentrations within the euphotic zone: A ubiquitous relationship. *Limnol Oceanogr* 45:1130–1143.
29. Morgan-Kiss RM, Priscu JC, Pocock T, Gudynaite-Savitch L, Huner NPA (2006) Adaptation and acclimation of photosynthetic microorganisms to permanently cold environments. *Microbiol Mol Biol Rev* 70:222–252.
30. Funder S, et al. (2011) A 10,000-year record of Arctic Ocean sea-ice variability—view from the beach. *Science* 333:747–750.
31. Billups K, Rickaby REM, Schrag DP (2004) Cenozoic pelagic Sr/Ca records: Exploring a link to paleoproductivity. *Paleoceanography*, 19:PA3005 10.1029/2004PA001011.
32. Vinther BM, et al. (2010) Climatic signals in multiple highly resolved stable isotope records from Greenland. *Quat Sci Rev* 29:522–538.
33. Belt ST, et al. (2010) Striking similarities in temporal changes to spring sea ice occurrence across the central Canadian Arctic Archipelago over the last 7000 years. *Quat Sci Rev* 29:3489–3504.
34. Veillette J, Mueller DR, Antoniades D, Vincent WF (2008) Arctic epishelf lakes as sentinel ecosystems: Past, present and future. *J Geophys Res* 113:G04014.
35. Gibson JAE, Trull T, Nichols PD, Summons RE, McMinn A (1999) Sedimentation of ^{13}C-rich organic matter from Antarctic sea-ice algae: A potential indicator of past sea-ice extent. *Geology* 27:331–334.
36. Domack E, et al. (2005) Stability of the Larsen B Ice Shelf on the Antarctic Peninsula during the Holocene epoch. *Nature* 436:681–685.

37. Bentley MJ, et al. (2005) Early Holocene retreat of the George VI Ice Shelf, Antarctic Peninsula. *Geology* 33:173–176.
38. Taylor F, Whitehead J, Domack E (2001) Holocene paleoclimate change in the Antarctic Peninsula: Evidence from the diatom, sedimentary and geochemical record. *Mar Micropaleontol* 41:25–43.
39. Pudsey CJ, Evans J (2001) First survey of Antarctic sub–ice shelf sediments reveals mid-Holocene ice shelf retreat. *Geology* 29:787–790.
40. Brachfield S, et al. (2003) Holocene history of the Larsen-A Ice Shelf constrained by geomagnetic paleointensity dating. *Geology* 31:749–752.
41. Zapata M, Rodriguez F, Garrido JL (2000) Separation of chlorophylls and carotenoids from marine phytoplankton: A new HPLC method using a reversed phase C8 column and pyridine-containing mobile phases. *Mar Ecol Prog Ser* 195:29–45.
42. Antoniades D, et al. (2010) Bacterial dominance of phototrophic communities in a High Arctic lake and its implications for paleoclimate analysis. *Polar Sci* 3:147–161.
43. Bennett KD (2008) Psimpoll (Queen's University Belfast, Belfast, UK) Version 4.26. Available online at http://www.chrono.qub.ac.uk/psimpoll/psimpoll.html.
44. Barletta F, St-Onge G, Channell JET, Rochon A (2010) Dating of Holocene western Canadian Arctic sediments by matching paleomagnetic secular variation to a geomagnetic field model. *Quat Sci Rev* 29:2315–2324.
45. Cook TL, Bradley RS, Stoner JS, Francus P (2009) Five thousand years of sediment transfer in a high arctic watershed recorded in annually laminated sediments from Lower Murray Lake, Ellesmere Island, Nunavut, Canada. *J Paleolimnol* 41: 77–94.
46. Korte M, Constable CG (2005) Continuous geomagnetic field models for the past 7 millennia: 2. CALS7K. *Geochem Geophys Geosyst* 6:Q02H16.
47. Reimer PJ, et al. (2009) Intcal9 and Marine09 radiocarbon age calibration curves, 0–50,000 years ka BP. *Radiocarbon* 51:1111–1150.
48. Coulthard RD, Furze MFA, Pienkowski AJ, Nixon FC, England JH (2010) New marine ΔR values for Arctic Canada. *Quat Geochronol* 5:419–434.
49. Hall BL, Henderson GM (2001) Use of uranium-thorium dating to determine past ^{14}C reservoir effects in lakes: Examples from Antarctica. *Earth Planet Sci Lett* 193:565–577.
50. Hendy CH, Hall BL (2006) The radiocarbon reservoir effect in proglacial lakes: Examples from Antarctica. *Earth Planet Sci Lett* 241:413–421.
51. Hattersley-Smith G (1963) The Ward Hunt Ice Shelf: Recent changes of the ice front. *J Glaciol* 4:415–424.
52. Bushnell VC (1956) Marvin's ice shelf journey, 1906. *Arctic* 9:166–177.
53. Vinther BM, et al. (2009) Holocene thinning of the Greenland ice sheet. *Nature* 461: 385–388.